ACS OMEGA

http://pubs.acs.org/journal/acsodf

Article

Large-Area Transfer of 2D TMDCs Assisted by a Water-Soluble Layer for Potential Device Applications

Madan Sharma, Aditya Singh, Pallavi Aggarwal, and Rajendra Singh*

Cite This: *ACS Omega* 2022, 7, 11731−11741

Read Online

ACCESS | Metrics & More | Article Recommendations | Supporting Information

ABSTRACT: Layer transfer offers enormous potential for the industrial implementation of two-dimensional (2D) material technology platforms. However, the transfer method used must retain the as-grown uniformity and cleanliness in the transferred films for the fabrication of 2D material-based devices. Additionally, the method used must be capable of large-area transfer to maintain wafer-scale fabrication standards. Here, a facile route to transfer centimeter-scale synthesized 2D transition metal dichalcogenides (TMDCs) (3L MoS_2, 1L WS_2) onto various substrates such as sapphire, SiO_2/Si, and flexible substrates (mica, polyimide) has been developed using a water-soluble layer (Na_2S/Na_2SO_4) underneath the as-grown film. The developed transfer process represents a fast, clean, generic, and scalable technique to transfer 2D atomic layers. The key strategy used in this process includes the dissolution of the Na_2S/Na_2SO_4 layer due to the penetration of NaOH solution between the growth substrate and hydrophobic 2D TMDC film. As a proof-of-concept device, a broadband photodetector has been fabricated onto the transferred 3L MoS_2, which shows photoresponse behavior for a wide range of wavelengths ranging from near-infrared (NIR) to UV. The enhancement in photocurrent was found to be 100 times and 10 times the dark current in the UV and visible regions, respectively. The fabricated photodetector shows a higher responsivity of 8.6 mA/W even at a low applied voltage (1.5 V) and low power density (0.6 μW/mm^2). The detector enables a high detectivity of 2.9×10^{11} Jones. This work opens up the pathway toward flexible electronics and optoelectronics.

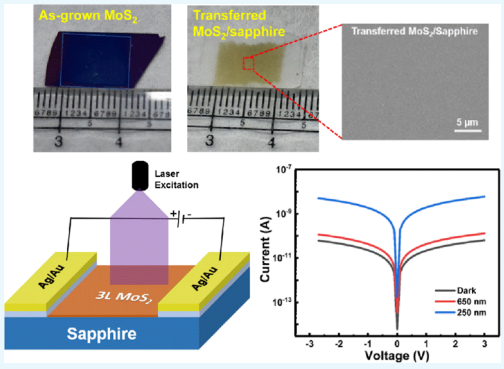

1. INTRODUCTION

Silicon-based electronic devices pose critical challenges in the sub-10 nm regime.[1] Rapid miniaturization of electronic devices needs exploration of new semiconducting materials. In the recent decade, two-dimensional (2D) transition metal dichalcogenides (TMDCs) are seen as a new hope for the electronic market due to their exotic mechanical, electrical, thermal, and optical properties.[2−4] Indirect to direct band gap cross-over of TMDCs from bulk to monolayers makes them suitable semiconducting materials for nanoscale electronic devices.[5] In the last few years, researchers have been optimistic that TMDCs could be the potential replacement of silicon (Si) in front-end-of-line (FEOL) technologies due to spectacular improvement in their performance. For example, the Hall mobility of 6L MoS_2 has been achieved up to 34 000 cm^2/(V s) at low temperature,[6] and the room temperature (RT) current on/off ratio of 1L MoS_2 can reach up to ∼10^8.[7] Initially, TMDC-based devices have been fabricated onto exfoliated flakes or some micrometer-sized flakes to optimize the material quality and device performance. However, the synthesis of large-area TMDCs is required to realize their commercial applications, so considerable efforts have been made to grow large-area 2D TMDCs.

Recently, Yang et al. have synthesized 6 inch large and uniform 1L MoS_2 by chemical vapor deposition (CVD) on soda−lime glass at a growth temperature of 720 °C.[8] However, the growth requirements for large-area, high-quality materials, namely high growth temperatures (>700 °C), the choice of substrates and precursors used for growth, etc., limit the potential applications.[9−11] Exemplifying this, the growth process negatively affects the underlying substrate at high temperatures, which degrades the performance of the fabricated devices.[12,13] In contrast, the growth temperature can be reduced by choosing appropriate precursors that avoid unwanted doping and contamination on the growth substrate.[14,15] Layer transfer of 2D TMDCs from the growth substrate to the application substrate is a viable approach to overcome these issues. Layer transfer is also needed for the fabrication of 2D/three-dimensional (3D) heterojunction-based devices[16−18] and flexible and transparent devices.[19,20] Due to the good optical transparency, high strain limit, and high surface area-to-volume ratio,[21,22] 2D TMDCs are

Received: December 4, 2021
Accepted: February 2, 2022
Published: April 2, 2022

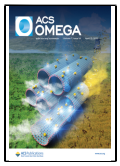

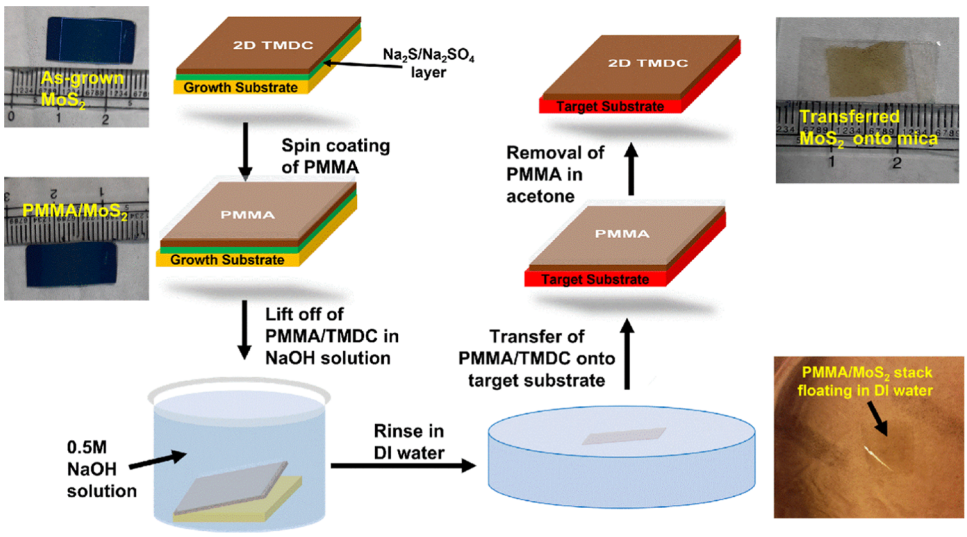

Figure 1. Schematic illustration of the water-soluble layer transfer process developed for MoS_2 and WS_2.

perfectly suited for use in flexible and wearable electronics and for Internet of things (IoT) applications.[15] Significant efforts have been made to transfer 2D material films without degrading the film quality, which is critical for the success of 2D materials.[23−28] In early studies, hazardous chemical etchants such as hydrofluoric acid (HF), hydrochloric acid (HCl), and nitric acid (HNO_3) were used to transfer 2D materials, which are environmentally unfriendly and degrade the film quality.[24,29] Strong bases such as KOH and NaOH have also been used to transfer the 2D material film, which are more attractive than hazardous chemical etchants.[30,31] However, these etchants degrade the film quality and device performance due to high corrosivity and dopping in the transferred film.[32] An ultrasonic bubbling transfer process[33] was also developed in which millions of microbubbles are generated by ultrasonication. These bubbles penetrate into the interface between the growth substrate and 2D film. However, this process is etchant-free but provides cracks and wrinkles on the transferred film due to the formation of bubbles at the film/substrate interface. Therefore, improvement and automation of layer transfer processes are needed for its industrial implementation.

In this work, we have developed a nondestructive, crack-free, and clean transfer technique based on the dissolution of the Na_2S/Na_2SO_4 layer. Although the Na_2S/Na_2SO_4 layer can be dissolved in DI water, we chose NaOH solution because cracks/wrinkles were observed on the film when it was transferred using pure DI water. To reduce the effect of the etchant on the transferred film, we took 0.5 M NaOH solution instead of 2 M solution. Trilayer (3L) MoS_2 and monolayer (1L) WS_2 have been transferred onto arbitrary substrates using this layer transfer method. Furthermore, we have demonstrated the fabrication of a photodetector onto the transferred 3L MoS_2 to show the potential of this process in device applications. The photodetector shows significant photoresponse for a wide range of wavelengths ranging from near-infrared (NIR) to UV. The photo-to-dark current ratio (PDCR) is 100 and 10 in the UV and visible (vis) region, respectively. Broadband photoresponse (NIR−vis−UV) of trilayer MoS_2 has been observed in this work. Furthermore, in most transfer methods, poly(methyl methacrylate) (PMMA) residues are not completely removed, which significantly impacts device performance. In the proposed process, PMMA residues were completely removed by putting the transferred film in an Ar flow of 480 sccm at 350 °C for 2 h.

2. RESULTS AND DISCUSSION

The complete layer transfer process is schematically illustrated in Figure 1. The substrate with as-grown 2D TMDCs was first spin-coated using PMMA for 120 s at a speed of 1000 rpm. The assembly was kept at room temperature (RT) overnight for better adhesion of PMMA and TMDC. Afterward, the complete assembly was dipped into a solution of 0.5 M NaOH. Before dipping into the solution, one edge of PMMA/TMDC was scratched so that the NaOH solution can easily penetrate from there to the interface of the growth substrate (GS) and TMDC. Within 1 min of dipping in the solution, the PMMA/TMDC stack started to lift off from the GS and float onto the surface of the solution. The lift-off process occurred as a result of the combined effect of the Na_2S/Na_2SO_4 layer dissolution and partial etching of SiO_2 by NaOH solution. The PMMA/TMDC stack was then rinsed in DI water to remove the contaminations from the NaOH solution and transferred onto the target substrate (TS). After that, the PMMA/TMDC/TS assembly was blown with N_2 gas to evaporate the water molecules and again kept overnight so that the transferred TMDC film gets better adhesion with TS. The hot acetone removed the PMMA, but still, there were some PMMA residues over the TMDC film. To remove these residues, the transferred film was placed in an Ar flow of 480 sccm at 350 °C for 2 h. Also, in this transfer process, we have selectively chosen 0.5 M NaOH solution for the lift-off instead of 2 M NaOH[30,31] and pure hot DI water. In 2 M NaOH solution, we observed that the transferred film was highly damaged due to the high corrosivity of the etchant (Figure S1). Similarly, when the complete PMMA/TMDC/TS stack was treated with hot DI water for lift-off, cracks and wrinkles were generated in the transferred film, worsening the film quality (Figure S2). Also, delamination of the PMMA/MoS_2 stack occurs at more than 15 min in water.

We can readily transfer large-area TMDCs using the aforementioned transfer process onto arbitrary substrates. To illustrate the viability of this process, we transferred centimeter-scale CVD-grown trilayer (3L) MoS_2 onto SiO_2/

https://doi.org/10.1021/acsomega.1c06855
ACS Omega 2022, 7, 11731−11741

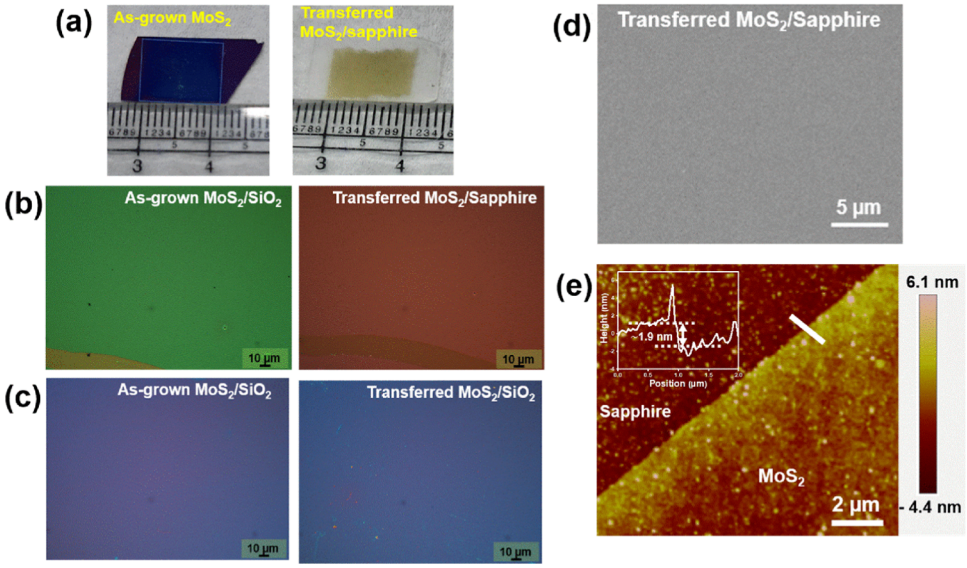

Figure 2. (a) Camera images of centimeter-scale as-grown and transferred 3L MoS_2. (b) Optical microscopy (OM) images of 3L MoS_2 synthesized on the SiO_2/Si substrate and MoS_2 transferred onto the sapphire substrate. (c) OM images of the as-synthesized 3L MoS_2/SiO_2 (GS) and transferred MoS_2/SiO_2 (TS). (d) SEM image of 3L MoS_2 transferred onto the sapphire substrate. (e) AFM image of transferred 3L MoS_2 onto the sapphire substrate. Inset: the thickness of 3L MoS_2 is shown by the height profile.

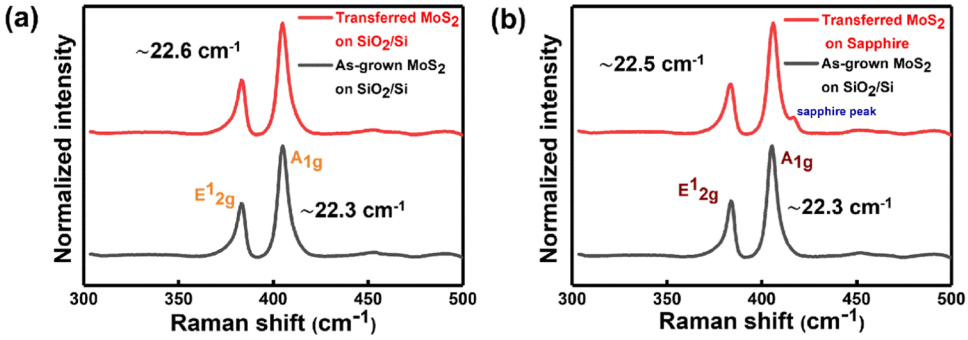

Figure 3. Raman spectra of 3L MoS_2 transferred from (a) SiO_2/Si (GS) to SiO_2/Si (TS) and (b) SiO_2/Si to the sapphire substrate.

Si and sapphire substrates. Figure 2a shows the transferred 3L MoS_2 film from SiO_2/Si to the sapphire substrate, which indicates the complete lift-off and release of the film from the GS. Through optical microscopy (OM), we observed that transferred films are clean, continuous, and uniform with no cracks and wrinkles (Figure 2b,c). Scanning electron microscopy (SEM) and atomic force microscopy (AFM) images further confirm the clean nature and uniformity of the transferred MoS_2 film. The SEM image clearly shows that the transferred 3L MoS_2 film is clean and wrinkle-free without polymer residues over it (Figure 2d). From the AFM analysis, it was observed that the surface roughness of the transferred 3L MoS_2 film was comparable to that of the as-grown film. The film thickness was measured to be around 1.9 nm from the line scan along the white line, confirming the trilayer nature of the MoS_2 film (Figure 2e).

We examined the optical quality of the transferred 3L MoS_2 using Raman spectroscopy, which is widely used to investigate the structural and layer properties of 2D materials.[34] Figure 3 depicts the Raman spectra of the as-synthesized and transferred 3L MoS_2 film. Raman spectra of MoS_2 consist of the two fundamental vibrational modes A_{1g} and E_{2g}^1, corresponding to out-of-plane and in-plane vibrations of atoms, respectively.[35] The peak position of these vibrational modes mainly depends on layer numbers and strain in the materials.[36,37] The frequency difference ($\Delta\omega$) between A_{1g} and E_{2g}^1 is an indicator of the number of layers in MoS_2. For the as-grown MoS_2, we observed that $\Delta\omega$ is 22.3 cm^{-1}, indicating that the MoS_2 film is trilayer in nature.[38] It is noteworthy that $\Delta\omega$ changes slightly from 22.3 to 22.6 and 22.3 to 22.5 cm^{-1} transferring the 3L MoS_2 film onto SiO_2/Si (TS) and the sapphire substrate, respectively (Figure 3a,b). This indicates that no strain was introduced in the film during the transfer process.[39] The small shift occurs due to the change in the interaction between the film and substrate rather than the change in layer numbers and the strain-induced one during the transfer. The as-grown film strongly interacts with the substrate as compared to the transferred film.[39] From the Raman and AFM measurements, it has been confirmed that no MoS_2 is left on the GS after the transfer, which ensures the complete lift-off of MoS_2 from the GS (Figures S3 and S4). From the AFM measurements, we have already confirmed that 3L MoS_2 remains as 3L after the transfer (Figure 2e).

We did XPS analysis of the as-grown and transferred 3L MoS_2 (GS−SiO_2/Si; TS−SiO_2/Si) to understand the effect of transfer on the stoichiometry and chemical composition of the MoS_2 film. Figure 4b shows the core-level spectra of Mo 3d and S 2s orbitals of the as-grown 3L MoS_2 film. The Mo^{+4} 3d

https://doi.org/10.1021/acsomega.1c06855
ACS Omega 2022, 7, 11731−11741

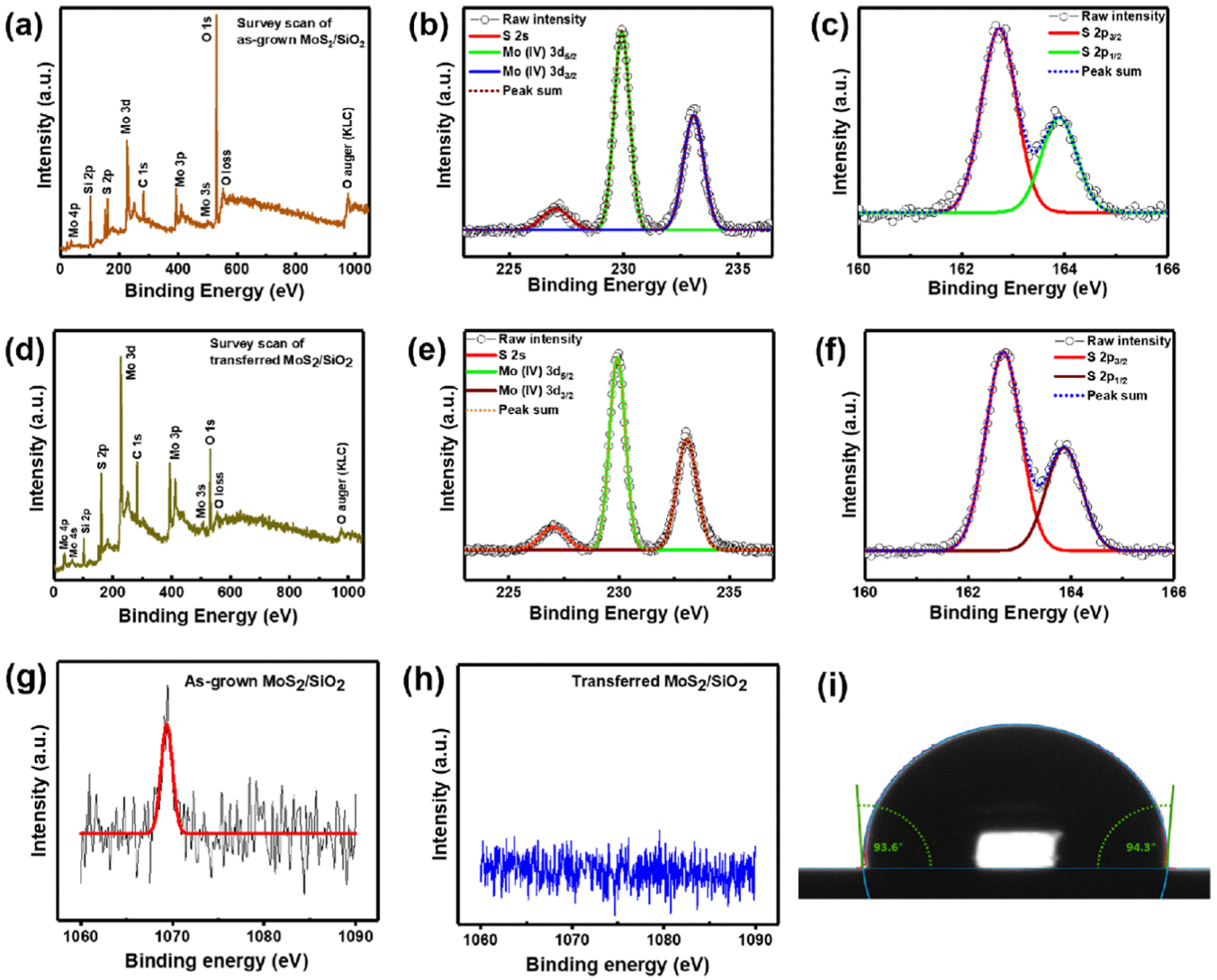

Figure 4. XPS spectra of 3L MoS_2 synthesized on SiO_2/Si (GS) and transferred onto SiO_2/Si (TS). (a, d) Survey spectrum of synthesized and transferred MoS_2, respectively. Core-level spectra of (b, e) Mo 3d and (c, f) S 2p peaks of as-grown and transferred MoS_2, respectively. (g) Na 1s binding energy spectrum of as-grown MoS_2 signifies the presence of the Na_2S/Na_2SO_4 layer underneath the MoS_2 film. (h) Na 1s peak was not observed in the transferred 3L MoS_2, confirming the dissolution of the Na_2S/Na_2SO_4 layer during the transfer process. (i) Contact angle measured for the transferred 3L MoS_2/SiO_2.

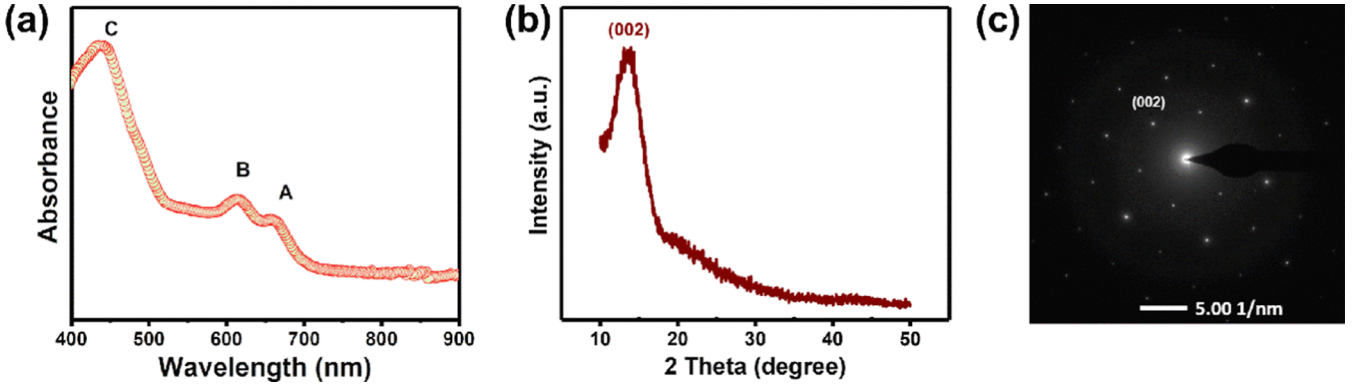

Figure 5. (a) UV−visible absorbance spectra and (b) XRD graph of transferred 3L MoS_2 onto the sapphire substrate. (c) SAED pattern showing the single-crystalline nature of 3L MoS_2.

spectra consist of two peaks centered at 229.8 and 233.0 eV, corresponding to $3d_{5/2}$ and $3d_{3/2}$, respectively. The full width at half maximum (FWHM) values of $3d_{5/2}$ and $3d_{3/2}$ peaks are ~0.65 and ~0.87 eV, respectively. A small hump at 227.0 eV in the spectra, in addition to the peaks of Mo 3d, corresponds to S 2s. The spectra of S 2p deconvoluted into two peaks of $2p_{3/2}$

https://doi.org/10.1021/acsomega.1c06855
ACS Omega 2022, 7, 11731−11741

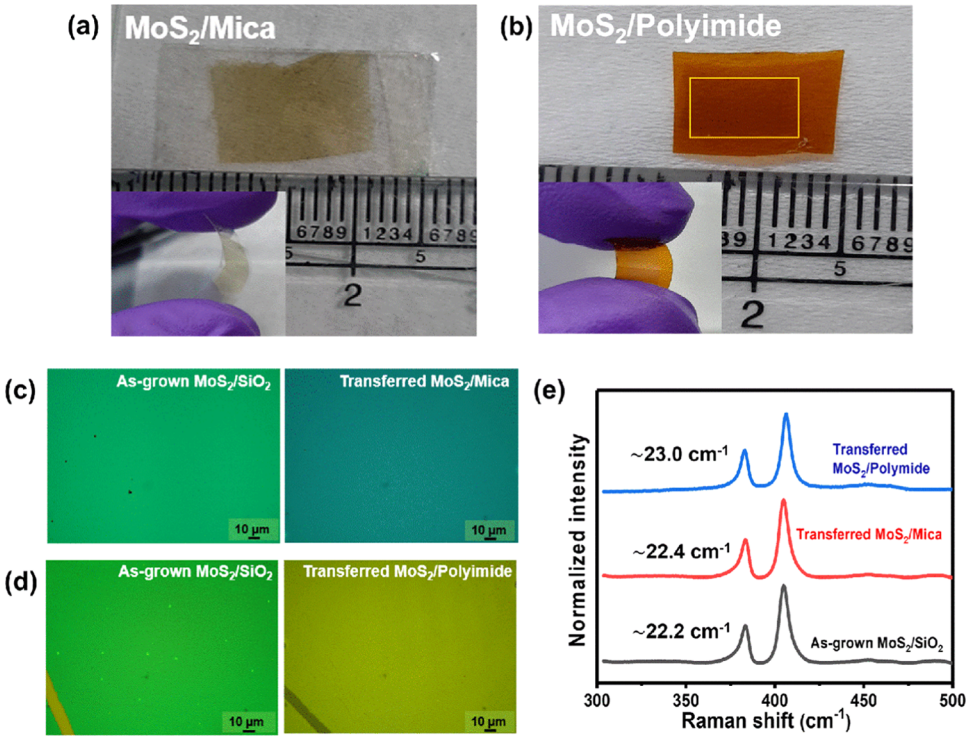

Figure 6. Photographs of the large-area (centimeter scale) transferred 3L MoS_2 film onto flexible (a) mica and (b) polyimide substrates. The insets of (a) and (b) show MoS_2/mica and MoS_2/polyimide bending, respectively. (c) OM images of as-synthesized 3L MoS_2/SiO_2 and transferred MoS_2/mica. (d) OM images of as-synthesized 3L MoS_2/SiO_2 and transferred MoS_2/polymide. (e) Raman spectra of as-grown and transferred 3L MoS_2 onto mica and polyimide substrates, respectively.

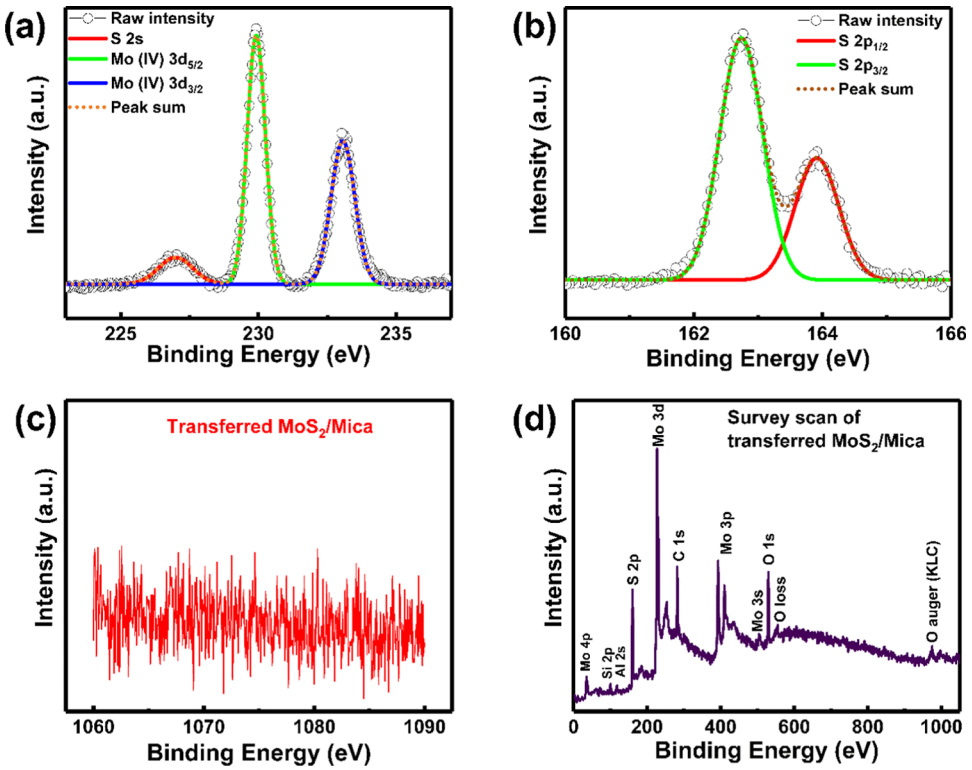

Figure 7. XPS spectra of core levels of (a) Mo 3d and (b) S 2p binding energies of transferred 3L MoS_2 onto the mica substrate. (c) No significance of the Na 1s peak in the transferred 3L MoS_2. (d) Survey scan of transferred 3L MoS_2/mica.

and $2p_{1/2}$, centered at 162.7 and 163.8 eV, with FWHM values of ~0.65 and ~0.68 eV, respectively (Figure 4c). All the values correctly match the previous literature reports.[40,41] As shown in Figure 4e,f, it has been observed that all the peak positions and FWHMs of the transferred film are almost similar to those of the as-grown film, indicating no change in the stoichiometry

https://doi.org/10.1021/acsomega.1c06855
ACS Omega 2022, 7, 11731−11741

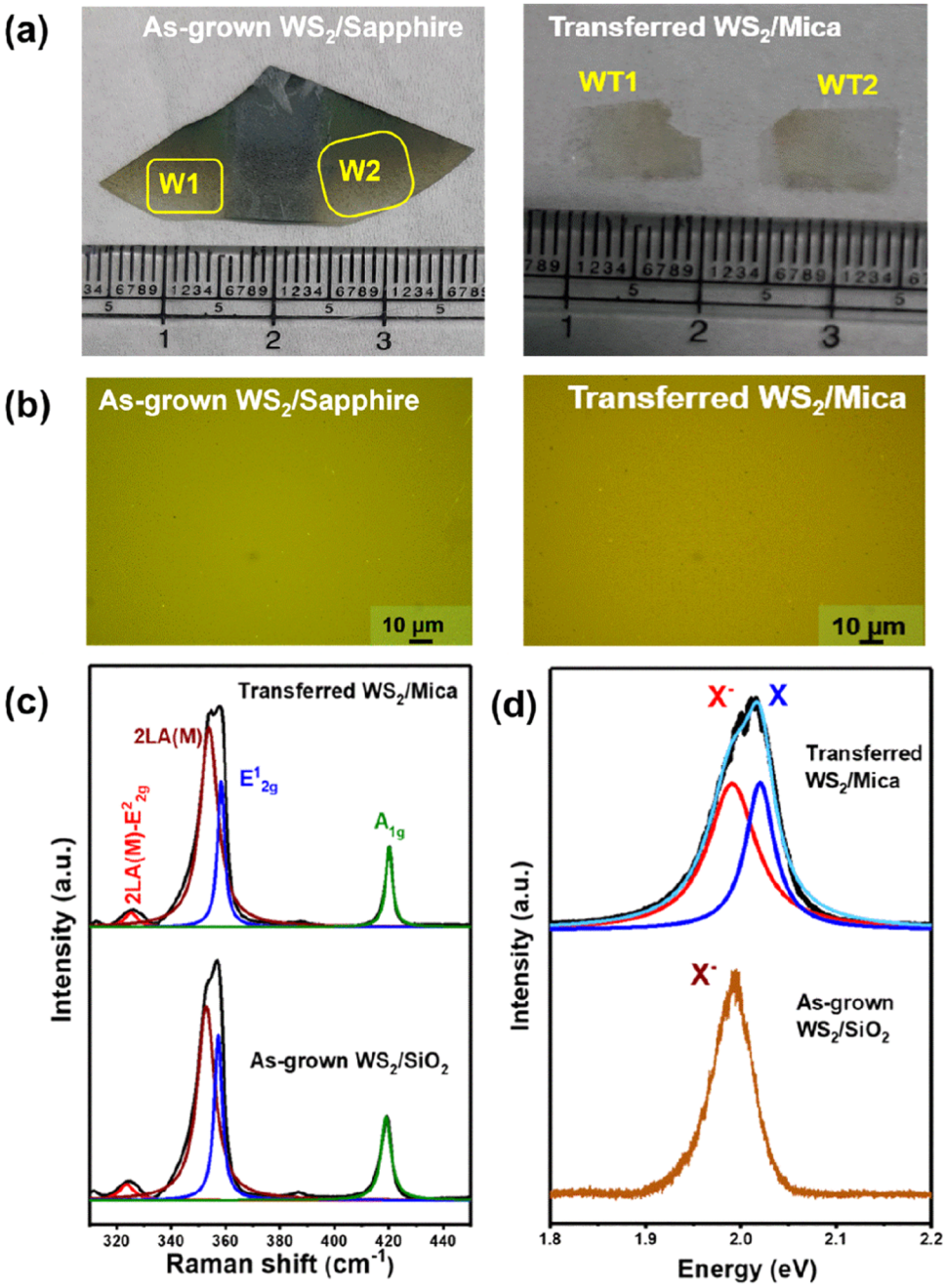

Figure 8. (a) Photographs of as-grown and transferred 1L WS_2 from sapphire to mica substrates. W1 and W2 are the monolayer regions of as-grown WS_2/sapphire. Similarly, WT1 and WT2 are the mica substrates onto monolayer. WS_2 was transferred from W1 and W2, respectively. (b) OM images of synthesized 1L WS_2/sapphire and transferred 1L WS_2/mica. (c) Raman and (d) PL measurement of as-grown and transferred WS_2.

and chemical composition of the 3L MoS_2 film after the transfer. The presence of Na_2S/Na_2SO_4 underneath the MoS_2 film was confirmed by Na 1s core-level spectra of the as-grown film positioned at 1071.2 eV[42,43] (Figure 4g). However, no Na 1s peak was observed in the transferred 3L MoS_2, confirming the dissolution of the Na_2S/Na_2SO_4 layer during the transfer process (Figure 4h). Figure 4i shows the water contact angle of transferred 3L MoS_2/SiO_2. The contact angle was around ~94.0°, which clearly shows the hydrophobic nature of MoS_2. The surface energy was calculated using the Fowkes model using the contact angles of diiodomethane and DI water.[44] The total surface energy of 3L MoS_2 was 35.72 mN/m, which is the sum of two components: polar component (0.72 mN/m) and dispersive component (35.00 mN/m). The dispersive component arises from the induced dipole−dipole interaction, and the polar component originates from the permanent dipole−dipole interaction.[45]

The optical properties and crystallinity of the transferred 3L MoS_2 film were investigated using UV−visible and X-ray diffraction (XRD) measurements on the transferred MoS_2/sapphire. In the UV−vis absorbance spectra of 3L MoS_2, we observed two prominent peaks at wavelengths 663 and 614 nm corresponding to A and B excitonic bands, respectively (Figure 5a). These two excitons get generated due to the direct transition between the conduction band minimum and the split valence band's maxima at the *K*-point of the Brillouin

https://doi.org/10.1021/acsomega.1c06855
ACS Omega 2022, 7, 11731−11741

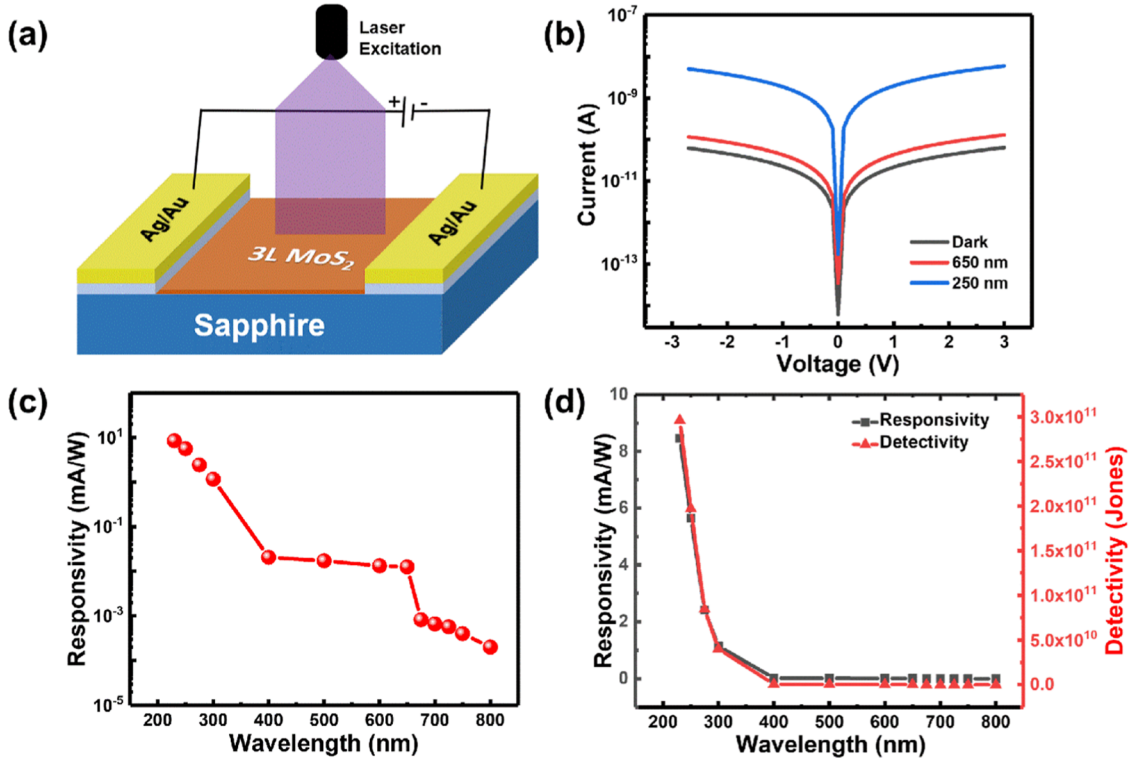

Figure 9. (a) Schematic illustration of the MSM photodetector with a monochromatic light beam. (b) $I-V$ characteristics of the photodetector in the dark and under 650 and 250 nm illuminating wavelengths. (c) Variation of responsivity of the device with illuminating wavelength ranging from UV to NIR. (d) Behavior of responsivity and detectivity with wavelength.

zone.[3,22] The absorbance peak (C exciton) around ∼440 nm was also observed, which corresponds to van Hove singularities in the electronic density of states of MoS_2.[36,46] As shown in Figure 5b, the XRD analysis of 3L MoS_2 shows a broad peak corresponding to the (002) plane at Bragg's angle $2\theta \approx 13.7°$. The XRD pattern matches the JCPDS card number 37-1492, confirming the hexagonal structure of MoS_2 with an interlayer spacing of 1.1 nm.[47] The selected area electron diffraction (SAED) pattern also ensures the single-crystalline nature and hexagonal symmetry of the 3L MoS_2 film (Figure 5c). Therefore, UV−visible spectroscopy and XRD confirm the high optical quality, uniformity, and single-crystalline nature of the large-area 3L MoS_2 film.

2.1. Transfer onto Flexible Substrates. To enhance the potential application of TMDCs in flexible electronics, we have transferred 3L MoS_2 onto flexible substrates: muscovite mica (highly flexible and high-temperature-stable) and polyimide. Optical microscopy images clearly show the clean and wrinkle-free transferred films (Figure 6c,d). From the Raman measurements shown in Figure 6e, we found that $\Delta\omega$ changes from 22.2 to 22.6 and 22.2 to 22.5 cm^{-1} for MoS_2 transferred onto mica and polyimide substrates, respectively. This again indicates that no strain was introduced in the film during the transfer process.[39] We also did the XPS analysis of the transferred 3L MoS_2/mica to confirm that our transfer process does not change the stoichiometry and chemical composition of the MoS_2 film. From Figure 7a,b, we observed no change in the peak positions and FWHM of peaks $3d_{5/2}$, $3d_{3/2}$, $2p_{3/2}$, and $2p_{1/2}$, which clearly shows that the stoichiometry and chemical composition of the transferred MoS_2 film are consistent with those of the as-grown film. The significance of the Na 1s peak was also not observed in the transferred MoS_2/mica sample (Figure 7c).

2.2. Layer Transfer of Large-Area Monolayer WS_2. To show the universality and feasibility of the transfer process, we implemented our transfer process to the transfer of large-area monolayer WS_2 from sapphire to mica substrates. Figure 8a shows an as-grown sample of 1L WS_2 on the sapphire substrate where W1 and W2 are the monolayer regions. The monolayer WS_2 film has been transferred from W1, W2 to WT1, and WT2 (WT1 and WT2 are mica substrates). The OM images shown in Figure 8b confirm the cleanliness of the transferred film. Raman and photoluminescence (PL) measurements were performed to examine the quality of transferred 1L WS_2. The Raman spectra of as-grown and transferred WS_2 are depicted in Figure 8c. Raman spectra contain two first-order vibrational modes: E_{2g}^1 (in-plane) and A_{1g} (out-of-plane) modes. We also observed two peaks at 324.1 and 352.5 cm^{-1} corresponding to 2LA(M)-E_{2g}^2 and 2LA(M) modes, respectively. The E_{2g}^1 mode of transferred WS_2 exhibits a blue shift of ∼1.5 cm^{-1} as compared to that of as-grown WS_2 due to the tensile strain release effect.[48] However, no shift was observed in the A_{1g} mode after the transfer because it was not impacted by strain. Conversely, the A_{1g} mode is susceptible to the charge doping effect, while the E_{2g}^1 mode is unaffected by charge doping because of the strong electron−phonon coupling.[49−51] In this transfer process, no additional charge doping was introduced; as a result, the A_{1g} mode of transferred and as-grown WS_2 remains identical. The 1L WS_2 shows the optical response from A and B excitonic transitions, which arise from the splitting of valence band maxima due to the spin−orbit interaction.[52,53] In the PL spectrum of as-grown 1L WS_2, a single peak was observed at 1.99 eV, which may contain both

https://doi.org/10.1021/acsomega.1c06855
ACS Omega 2022, 7, 11731−11741

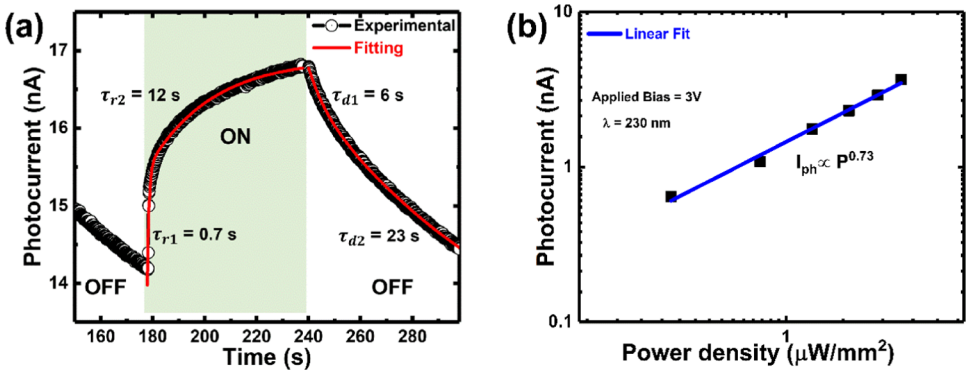

Figure 10. (a) Temporal response of the device recorded at 5 V biased voltage and fitted with the biexponential equation. The device was exposed to light for a period of 100 s, and then, the light was turned off for 100 s. (b) Linear response of photocurrent with incident power density.

charged (X^- and X^+ trions) and neutral (X) A excitons (Figure 8d). The B excitonic peak is not measurable with this laser excitation. The PL spectrum of transferred WS_2 clearly shows the two distinct components neutral exciton (X) at 2.02 eV and negatively charged trion (X^-) at 1.99 eV, which are well-fitted by the Lorentzian function. Note that the neutral exciton is fully absent in as-grown WS_2, while the X^- trion peak of transferred WS_2 is very similar to that of as-grown WS_2.[50] The suppression of the neutral excitonic peak in as-grown WS_2 is due to the unintentional doping of electrons from the water-soluble layer underneath WS_2 and the n-type semiconducting nature of WS_2. The water-soluble layer was completely dissolved during the transfer, reducing the unintended electron doping in WS_2.[26] This is the reason for that the intensity of the X exciton dominates the intensity of the X^- trion in the PL spectrum of transferred WS_2. Raman and PL spectra confirm that 1L WS_2 retains its optical properties after the transfer.

2.3. Device Application of the Water-Soluble Transfer Method. The compatibility of this transfer method with the nanoscale device fabrication technology was demonstrated by fabricating a broadband photodetector onto the transferred 3L MoS_2/sapphire. The typical schematic of a metal−semiconductor−metal (MSM) photodetector is shown in Figure 9a. The electrical contacts of Ag/Au (40/60 nm) were deposited onto the MoS_2 film by thermal evaporation using a metal mask. The photo-to-dark current ratio (PDCR), responsivity (R), detectivity (D^*), and response time (t_{res}) are the key parameters for the performance of a photodetector. PDCR, R, and D^* are defined as

$$\text{PDCR} = \frac{I_p}{I_d} \tag{1}$$

$$R = \frac{I_p - I_d}{P_\lambda A_{eff}} \tag{2}$$

$$D^* = \sqrt{\frac{A_{eff}}{2eI_d}} \times R \tag{3}$$

where I_d and I_p are the dark current and photocurrent, respectively, the power density is symbolized by P_λ corresponding to wavelength λ, A_{eff} is the effective area of the device illuminated with light, which is found to be 4.9 mm^2 for the present case, and e is the unit charge. Figure 9b shows the room temperature dark and photocurrent at wavelengths of 250 and 650 nm with power densities of 1 and 23.34 $\mu W/mm^2$, respectively. A significant increase can be seen in the photocurrent upon illumination of light. Interestingly, the photocurrent increased 10 times the dark current for the wavelength of 650 nm (visible region), while it increased 100 times for the wavelength of 250 nm (UV region). The enhancement in the current can be attributed to the generation of electron−hole pairs when the device is exposed to light under a biasing voltage. Figure 9c shows the spectral responsivity measurements carried out from 230 to 800 nm wavelengths at a fixed applied voltage (1.5 V). Responsivity continuously increases with a decrease in the illuminated wavelength. At a wavelength of 800 nm (NIR region) corresponding to the band gap of ~1.5 eV of trilayer MoS_2, the device shows weak photoresponse because the power density used here is very small (12.65 $\mu W/mm^2$). As reported by Choi et al., high power density is required for the noticeable photoresponse at the wavelength of 800 nm due to the weak absorption tail of the indirect band gap transition.[54] The first significant increase in responsivity was observed at 650 nm, corresponding to the band gap of monolayer MoS_2. However, responsivity is significantly increased in the UV region compared to that in the visible region, and the maximum value of R is 8.6 mA/W even at a low applied voltage (1.5 V) and low power density (0.6 $\mu W/mm^2$). The obtained responsivity value at a relatively low applied voltage is higher than that of some of the previously reported UV photodetectors based on 2D materials.[54−56] Figure 9d shows the calculated D^* of photodetector at different wavelengths. The maximum detectivity was found to be 2.9×10^{11} Jones, which is comparatively higher than that of some of the previously reported photodetector devices.[57−60]

Furthermore, the temporal response was taken to evaluate the detection speed of the photodetector. We have measured the time-dependent photocurrent at 3 V under UV illumination of 230 nm wavelength. The following biexponential equation was fitted with experimental data of the time−response curve to analyze the fast and slow components of the rise and decay times.[61]

$$I = I_0 + A_1 e^{-t/\tau_1} + A_2 e^{-t/\tau_2} \tag{4}$$

where I is the current at any time t. I_0 is steady-state current, A_1 and A_2 are fitting constants, and τ_1 and τ_2 are relaxation time constants. The fast (slow) components of the rise time were denoted by τ_{r1} (τ_{r2}). The fast and slow decay time components were denoted by τ_{d1} and τ_{d2}, respectively. Figure 10a shows the time-dependent photoresponse curve fitted with the biexponential eq 4. The fast and slow components of rise time were

https://doi.org/10.1021/acsomega.1c06855
ACS Omega 2022, 7, 11731−11741

found to be 0.7 and 12 s, respectively. Also, fast and slow decay components were extracted as 6 and 23 s, respectively. The decay time of current is relatively slow compared to the rise time, which may be due to the presence of traps and vacancies in the material.[62] In addition, power density-dependent photoresponse was also investigated, and photocurrent was fitted with the power law.[63]

$$I_p = aP_\lambda^{\ b} \tag{5}$$

where P_λ is the power density and a and b are the proportionality constant and empirical constant, respectively. $b = 1$ indicates the trap-free carrier transport, and $b < 1$ suggests the trap-influenced carrier transport in the material. At 3 V applied voltage and 230 nm wavelength, b was found to be 0.73, showing the trap-assisted photocurrent transport (Figure 10b). Hence, the present work paves the way to utilize the 2D TMDCs for nanodevice fabrication.

3. CONCLUSIONS

In summary, we have demonstrated a water-soluble layer-based transfer method enabling the clean transfer of large-area (centimeter scale) CVD-grown 2D TMDCs onto arbitrary substrates, including flexible substrates such as mica and polyimide. The preservation of the crystalline quality of the transferred film was confirmed by performing various characterization techniques. The versatility of the transfer method has been shown by transferring 3L MoS_2 and 1L WS_2 onto different substrates. Large-area transfer of TMDCs onto flexible substrates (mica, polyimide) allows the fabrication of flexible devices. This water-soluble layer-based transfer technique can be a good alternative to the wet-etching transfer method. The photodetector fabricated onto transferred 3L MoS_2 shows the compatibility of this transfer method with the nanoscale device fabrication technology. In addition, the photodetector exhibits broadband photoresponse (NIR−vis−UV) with a maximum responsivity of 8.6 mA/W and detectivity of 2.9×10^{11} Jones. The photocurrent significantly increased 100 times the dark current in the UV region, while it increased 10 times in the visible region. This work will serve the interest of the research community working toward the manufacturing of devices based on 2D materials for electronics, optoelectronics, bioinspired electronics, and flexible electronics. This transfer process can also integrate 2D materials with various platforms such as Si augmentation/replacement, IoT, and 2D/2D heterostructures.

4. EXPERIMENTAL SECTION

4.1. Synthesis of Large-Area Trilayer MoS_2. A single-zone atmospheric pressure chemical vapor deposition (APCVD) system with a long quartz tube (45 cm) having 5 cm diameter was used to achieve the large-area synthesis of trilayer (3L) MoS_2 over the SiO_2 (300 nm, thermally oxidized Si)/Si substrate. Before the synthesis, the tube was purged at 300 °C with a 480 sccm argon (Ar) gas flow for 10 min to remove the preoccupied precursors, moisture, and other contaminations. In the typical procedure, we have chosen a molybdenum trioxide (MoO_3)-to-sulfur (S) particle ratio of ∼1:30 (MoO_3 = 15 mg, S = 100 mg). For the growth of MoS_2, 100 mg of NaCl powder was mixed with MoO_3 powder in a quartz boat and placed in the middle of the CVD furnace tube. Another boat was placed 13.5 cm away from the middle of the tube, which contains S powder. MoS_2 was successfully grown at 650 °C for 20 min. Large-area growth of 3L-MoS_2 was achieved by controlling the concentration boundary layer formation in NaCl-assisted CVD of MoS_2. The concentration boundary layer is composed of sulfur and MoO_3 reactants, which react in a gaseous phase under the influence of NaCl powder. However, to investigate the role of the concentration boundary layer in CVD growth, we have tuned the distance between MoO_3 + NaCl precursors and the growing substrate. We have synthesized a high-quality large-area (centimeter scale) 3L-MoS_2 film over the SiO_2/Si substrate with good repeatability in synthesis. As reported in our previous work, a water-soluble layer (Na_2S/Na_2SO_4) was also grown underneath MoS_2.[42,64] The Na_2S/Na_2SO_4 layer functions as a seed promoter and supports the nucleation of the large-area, uniform, and continuous MoS_2 film.

4.2. Synthesis of Large-Area Monolayer WS_2. The same single-zone APCVD system was used to grow the large-area monolayer (1L) WS_2 over the sapphire substrate. The tube was purged at 150 °C with a 480 sccm Ar gas flow for 30 min to remove humidity and the predeposited contaminants. A mixture of NaCl and WO_3 (99.995%, Sigma-Aldrich, 204781) powder was placed in the middle of the CVD furnace for 1 min at 820 °C, and 200 mg of sulfur (99.98%, Sigma-Aldrich, 414980) was placed at 20 cm away from the center of the furnace to achieve sulfurization in a 120 sccm Ar gas flow environment.

4.3. Characterization Techniques. We have performed photoluminescence (PL) and Raman measurements at room temperature (RT) using a Horiba Scientific (LabRAM HR Evolution) with 514 nm laser wavelength to study the optical properties of 3L MoS_2 and 1L WS_2 films. To analyze the surface morphology and thickness of the film, atomic force microscopy (AFM) was performed using a Bruker (Dimension ICON). A monochromatic Al Kα X-ray line (probe size ∼1.7 mm × 2.7 mm energy 1486.7 eV) was used for X-ray photoelectron spectroscopy (XPS) analysis. A Philips Xpert Pro system with Cu Kα (λ = 1.54 Å) was used to perform the X-ray diffraction (XRD) measurements. An FESEM−Zeiss microscope (backscattering mode) was used to perform field emission scanning electron microscopy (FESEM). The photocurrent measurements were performed using a DC probe station (EverBeingEB6) coupled with a Keithley semiconductor characterization system (SCS4200). A xenon lamp (75 W) was used to measure the photoresponse of the device, which is combined with a computer-interfaced monochromator (Bentham TMC-300V). A Thorlabs power meter (PM-100D) was used for the power spectrum of the xenon lamp.

■ ASSOCIATED CONTENT

Supporting Information

The Supporting Information is available free of charge at https://pubs.acs.org/doi/10.1021/acsomega.1c06855.

Transfer of 3L MoS_2 in 2 M NaOH solution, optical image of transferred 3L MoS_2 lifted off in hot DI water, optical and AFM images of the as-grown sample after transfer, and Raman spectra of the as-grown sample after transfer (PDF)

https://doi.org/10.1021/acsomega.1c06855
ACS Omega 2022, 7, 11731−11741

AUTHOR INFORMATION

Corresponding Author

Rajendra Singh − *Department of Physics, Indian Institute of Technology Delhi, New Delhi 110016, India; Department of Electrical Engineering and Nanoscale Research Facility, Indian Institute of Technology Delhi, New Delhi 110016, India;* orcid.org/0000-0002-6890-6904; Email: rsingh@physics.iitd.ac.in

Authors

Madan Sharma − *Department of Physics, Indian Institute of Technology Delhi, New Delhi 110016, India*

Aditya Singh − *Department of Physics, Indian Institute of Technology Delhi, New Delhi 110016, India;* orcid.org/0000-0002-4301-1397

Pallavi Aggarwal − *Department of Physics, Indian Institute of Technology Delhi, New Delhi 110016, India*

Complete contact information is available at: https://pubs.acs.org/10.1021/acsomega.1c06855

Notes

The authors declare no competing financial interest.

ACKNOWLEDGMENTS

Madan Sharma thanks the Department of Science and Technology (DST) for the award of the research fellowship. The authors acknowledge the Nanoscale Research Facility (NRF) and Central Research Facility (CRF), Indian Institute of Technology Delhi, New Delhi, for providing the characterization facilities. We would also like to acknowledge "Grand Challenge Project on MBE growth of 2D materials" sponsored by the Ministry of Human Resource Development (MHRD), India, and IIT Delhi for partial financial support for this work.

REFERENCES

(1) Haron, N. Z.; Hamdioui, S. In *Why is CMOS scaling coming to an END?* 2008 3rd International Design and Test Workshop; IEEE, 2008; pp 98−103.

(2) Duong, D. L.; Yun, S. J.; Lee, Y. H. van der Waals layered materials: Opportunities and challenges. *ACS Nano* **2017**, *11*, 11803−11830.

(3) Mak, K. F.; Lee, C.; Hone, J.; Shan, J.; Heinz, T. F. Atomically thin MoS2: a new direct-gap semiconductor. *Phys. Rev. Lett.* **2010**, *105*, No. 136805.

(4) Wang, Q. H.; Kalantar-Zadeh, K.; Kis, A.; Coleman, J. N.; Strano, M. S. Electronics and optoelectronics of two-dimensional transition metal dichalcogenides. *Nat. Nanotechnol.* **2012**, *7*, 699−712.

(5) Xu, M.; Liang, T.; Shi, M.; Chen, H. Graphene-like two-dimensional materials. *Chem. Rev.* **2013**, *113*, 3766−3798.

(6) Cui, X.; Lee, G.-H.; Kim, Y. D.; Arefe, G.; Huang, P. Y.; Lee, C.-H.; Chenet, D. A.; Zhang, X.; Wang, L.; Ye, F.; et al. Multi-terminal transport measurements of MoS2 using a van der Waals heterostructure device platform. *Nat. Nanotechnol.* **2015**, *10*, 534−540.

(7) Radisavljevic, B.; Radenovic, A.; Brivio, J.; Giacometti, V.; Kis, A. Single-layer MoS2 transistors. *Nat. Nanotechnol.* **2011**, *6*, 147−150.

(8) Yang, P.; Zou, X.; Zhang, Z.; Hong, M.; Shi, J.; Chen, S.; Shu, J.; Zhao, L.; Jiang, S.; Zhou, X.; et al. Batch production of 6-inch uniform monolayer molybdenum disulfide catalyzed by sodium in glass. *Nat. Commun.* **2018**, *9*, No. 979.

(9) Xie, Y.; Wang, G.; Wang, Z.; Nan, T.; Wang, H.; Wang, Y.; Zhan, Y.; Jie, W.; Ma, X. Growth of Monolayer WS 2 Single Crystals with Atmospheric Pressure CVD: Role of Temperature. *MRS Adv.* **2019**, *4*, 255−262.

(10) Özden, A.; Ay, F.; Sevik, C.; Perkgöz, N. K. CVD growth of monolayer MoS2: role of growth zone configuration and precursors ratio. *Jpn. J. Appl. Phys.* **2017**, *56*, No. 06GG05.

(11) Choudhury, T. H.; Zhang, X.; Balushi, Z. Y. A.; Chubarov, M.; Redwing, J. M. Epitaxial Growth of Two-Dimensional Layered Transition Metal Dichalcogenides. *Annu. Rev. Mater. Res.* **2020**, *50*, 155−177.

(12) Kalanyan, B.; Kimes, W. A.; Beams, R.; Stranick, S. J.; Garratt, E.; Kalish, I.; Davydov, A. V.; Kanjolia, R. K.; Maslar, J. E. Rapid wafer-scale growth of polycrystalline 2H-MoS2 by pulsed metal−organic chemical vapor deposition. *Chem. Mater.* **2017**, *29*, 6279−6288.

(13) Mandyam, S. V.; Kim, H. M.; Drndić, M. J. Large area few-layer TMD film growths and their applications. *J. Phys.: Mater.* **2020**, *3*, No. 024008.

(14) Li, H.; Li, Y.; Aljarb, A.; Shi, Y.; Li, L.-J. Epitaxial growth of two-dimensional layered transition-metal dichalcogenides: growth mechanism, controllability, and scalability. *Chem. Rev.* **2018**, *118*, 6134−6150.

(15) Briggs, N.; Subramanian, S.; Lin, Z.; Li, X.; Zhang, X.; Zhang, K.; Xiao, K.; Geohegan, D.; Wallace, R.; Chen, L.-Q.; et al. A roadmap for electronic grade 2D materials. *2D Mater.* **2019**, *6*, No. 022001.

(16) Walsh, L. A.; Hinkle, C. L. van der Waals epitaxy: 2D materials and topological insulators. *Appl. Mater. Today* **2017**, *9*, 504−515.

(17) Addou, R.; Wallace, R. M. Integration of 2D materials for advanced devices: challenges and opportunities. *ECS Trans.* **2017**, *79*, No. 11.

(18) Kozhakhmetov, A.; Nasr, J. R.; Zhang, F.; Xu, K.; Briggs, N. C.; Addou, R.; Wallace, R.; Fullerton-Shirey, S. K.; Terrones, M.; Das, S.; et al. Scalable BEOL compatible 2D tungsten diselenide. *2D Mater.* **2020**, *7*, No. 015029.

(19) Roselli, L.; Carvalho, N. B.; Alimenti, F.; Mezzanotte, P.; Orecchini, G.; Virili, M.; Mariotti, C.; Goncalves, R.; Pinho, P. J. P. oti. Smart surfaces: Large area electronics systems for Internet of Things enabled by energy harvesting. *Proc. IEEE* **2014**, *102*, 1723−1746.

(20) Zhan, Y.; Mei, Y.; Zheng, L. J. Materials capability and device performance in flexible electronics for the Internet of Things. *J. Mater. Chem. C* **2014**, *2*, 1220−1232.

(21) Korn, T.; Heydrich, S.; Hirmer, M.; Schmutzler, J.; Schüller, C. Low-temperature photocarrier dynamics in monolayer MoS2. *Appl. Phys. Lett.* **2011**, *99*, No. 102109.

(22) Splendiani, A.; Sun, L.; Zhang, Y.; Li, T.; Kim, J.; Chim, C.-Y.; Galli, G.; Wang, F. Emerging photoluminescence in monolayer MoS2. *Nano Lett.* **2010**, *10*, 1271−1275.

(23) Cho, H.-Y.; Nguyen, T. K.; Ullah, F.; Yun, J.-W.; Nguyen, C. K.; Kim, Y. S. Salt-assisted clean transfer of continuous monolayer MoS2 film for hydrogen evolution reaction. *Phys. B* **2018**, *532*, 84−89.

(24) Elías, A. L.; Perea-López, N.; Castro-Beltrán, A.; Berkdemir, A.; Lv, R.; Feng, S.; Long, A. D.; Hayashi, T.; Kim, Y. A.; Endo, M.; et al. Controlled synthesis and transfer of large-area WS2 sheets: from single layer to few layers. *ACS Nano* **2013**, *7*, 5235−5242.

(25) Lai, S.; Jeon, J.; Song, Y.-J.; Lee, S. Water-penetration-assisted mechanical transfer of large-scale molybdenum disulfide onto arbitrary substrates. *RSC Adv.* **2016**, *6*, 57497−57501.

(26) Sharma, M.; Singh, A.; Singh, R. Monolayer MoS2 Transferred on Arbitrary Substrates for Potential Use in Flexible Electronics. *ACS Appl. Nano Mater.* **2020**, *3*, 4445−4453.

(27) Zhang, F.; Erb, C.; Runkle, L.; Zhang, X.; Alem, N. Etchant-free transfer of 2D nanostructures. *Nanotechnology* **2017**, *29*, No. 025602.

(28) Schranghamer, T. F.; Sharma, M.; Singh, R.; Das, S. Review and comparison of layer transfer methods for two-dimensional materials for emerging applications. *Chem. Soc. Rev.* **2021**, *50*, 11032−11054.

(29) Reina, A.; Jia, X.; Ho, J.; Nezich, D.; Son, H.; Bulovic, V.; Dresselhaus, M. S.; Kong, J. Large area, few-layer graphene films on arbitrary substrates by chemical vapor deposition. *Nano Lett.* **2009**, *9*, 30−35.

(30) Wang, X.; Gong, Y.; Shi, G.; Chow, W. L.; Keyshar, K.; Ye, G.; Vajtai, R.; Lou, J.; Liu, Z.; Ringe, E.; et al. Chemical vapor deposition growth of crystalline monolayer MoSe2. *ACS Nano* **2014**, *8*, 5125−5131.
(31) Lin, Y.-C.; Zhang, W.; Huang, J.-K.; Liu, K.-K.; Lee, Y.-H.; Liang, C.-T.; Chu, C.-W.; Li, L.-J. Wafer-scale MoS 2 thin layers prepared by MoO 3 sulfurization. *Nanoscale* **2012**, *4*, 6637−6641.
(32) Amani, M.; Chin, M. L.; Mazzoni, A. L.; Burke, R. A.; Najmaei, S.; Ajayan, P. M.; Lou, J.; Dubey, M. Growth-substrate induced performance degradation in chemically synthesized monolayer MoS2 field effect transistors. *Appl. Phys. Lett.* **2014**, *104*, No. 203506.
(33) Ma, D.; Shi, J.; Ji, Q.; Chen, K.; Yin, J.; Lin, Y.; Zhang, Y.; Liu, M.; Feng, Q.; Song, X.; et al. A universal etching-free transfer of MoS 2 films for applications in photodetectors. *Nano Res.* **2015**, *8*, 3662−3672.
(34) Lin, Z.; Carvalho, B. R.; Kahn, E.; Lv, R.; Rao, R.; Terrones, H.; Pimenta, M. A.; Terrones, M. Defect engineering of two-dimensional transition metal dichalcogenides. *2D Mater.* **2016**, *3*, No. 022002.
(35) Korn, T.; Heydrich, S.; Hirmer, M.; Schmutzler, J.; Schüller, C. Low-temperature photocarrier dynamics in monolayer MoS2. *Appl. Phys. Lett.* **2011**, *99*, No. 102109.
(36) Dumcenco, D.; Ovchinnikov, D.; Marinov, K.; Lazic, P.; Gibertini, M.; Marzari, N.; Sanchez, O. L.; Kung, Y.-C.; Krasnozhon, D.; Chen, M.-W.; et al. Large-area epitaxial monolayer MoS2. *ACS Nano* **2015**, *9*, 4611−4620.
(37) Chae, W. H.; Cain, J. D.; Hanson, E. D.; Murthy, A. A.; Dravid, V. P. Substrate-induced strain and charge doping in CVD-grown monolayer MoS2. *Appl. Phys. Lett.* **2017**, *111*, No. 143106.
(38) Li, H.; Wu, J.; Yin, Z.; Zhang, H. Preparation and applications of mechanically exfoliated single-layer and multilayer MoS2 and WSe2 nanosheets. *Acc. Chem. Res.* **2014**, *47*, 1067−1075.
(39) Buscema, M.; Steele, G. A.; van der Zant, H. S.; Castellanos-Gomez, A. The effect of the substrate on the Raman and photoluminescence emission of single-layer MoS2. *Nano Res.* **2014**, *7*, 561−571.
(40) Mukherjee, S.; Maiti, R.; Midya, A.; Das, S.; Ray, S. K. Tunable direct bandgap optical transitions in MoS2 nanocrystals for photonic devices. *ACS Photonics* **2015**, *2*, 760−768.
(41) Kim, I. S.; Sangwan, V. K.; Jariwala, D.; Wood, J. D.; Park, S.; Chen, K.-S.; Shi, F.; Ruiz-Zepeda, F.; Ponce, A.; Jose-Yacaman, M.; et al. Influence of stoichiometry on the optical and electrical properties of chemical vapor deposition derived MoS2. *ACS Nano* **2014**, *8*, 10551−10558.
(42) Singh, A.; Moun, M.; Sharma, M.; Barman, A.; Kapoor, A. K.; Singh, R. NaCl-assisted substrate dependent 2D planar nucleated growth of MoS2. *Appl. Surf. Sci.* **2021**, *538*, No. 148201.
(43) Song, J.-G.; Ryu, G. H.; Kim, Y.; Woo, W. J.; Ko, K. Y.; Kim, Y.; Lee, C.; Oh, I.-K.; Park, J.; Lee, Z.; et al. Catalytic chemical vapor deposition of large-area uniform two-dimensional molybdenum disulfide using sodium chloride. *Nanotechnology* **2017**, *28*, No. 465103.
(44) Fowkes, F. M. J. T. Additivity of intermolecular forces at interfaces. i. determination of the contribution to surface and interfacial tensions of dispersion forces in various liquids1. *J. Phys. Chem. A* **1963**, *67*, 2538−2541.
(45) Annamalai, M.; Gopinadhan, K.; Han, S. A.; Saha, S.; Park, H. J.; Cho, E. B.; Kumar, B.; Patra, A.; Kim, S.-W.; Venkatesan, T. Surface energy and wettability of van der Waals structures. *Nanoscale* **2016**, *8*, 5764−5770.
(46) Britnell, L.; Ribeiro, R. M.; Eckmann, A.; Jalil, R.; Belle, B.; Mishchenko, A.; Kim, Y.-J.; Gorbachev, R.; Georgiou, T.; Morozov, S. V. Strong light-matter interactions in heterostructures of atomically thin films. *Science* **2013**, *340*, 1311−1314.
(47) Gomathi, P. T.; Sahatiya, P.; Badhulika, S. Large-area, flexible broadband photodetector based on ZnS−MoS2 hybrid on paper substrate. *Adv. Funct. Mater.* **2017**, *27*, No. 1701611.
(48) McCreary, K. M.; Hanbicki, A. T.; Singh, S.; Kawakami, R. K.; Jernigan, G. G.; Ishigami, M.; Ng, A.; Brintlinger, T. H.; Stroud, R. M.; Jonker, B. T. The effect of preparation conditions on Raman and photoluminescence of monolayer WS2. *Sci. Rep.* **2016**, *6*, No. 35154.
(49) Ahn, G. H.; Amani, M.; Rasool, H.; Lien, D.-H.; Mastandrea, J. P.; Ager, J. W., III; Dubey, M.; Chrzan, D. C.; Minor, A. M.; Javey, A. Strain-engineered growth of two-dimensional materials. *Nat. Commun.* **2017**, *8*, No. 608.
(50) Peimyoo, N.; Yang, W.; Shang, J.; Shen, X.; Wang, Y.; Yu, T. Chemically driven tunable light emission of charged and neutral excitons in monolayer WS2. *ACS Nano* **2014**, *8*, 11320−11329.
(51) Chakraborty, B.; Bera, A.; Muthu, D.; Bhowmick, S.; Waghmare, U. V.; Sood, A. Symmetry-dependent phonon renormalization in monolayer MoS 2 transistor. *Phys. Rev. B* **2012**, *85*, No. 161403.
(52) Zhao, W.; Ghorannevis, Z.; Chu, L.; Toh, M.; Kloc, C.; Tan, P.-H.; Eda, G. Evolution of electronic structure in atomically thin sheets of WS2 and WSe2. *ACS Nano* **2013**, *7*, 791−797.
(53) Peimyoo, N.; Shang, J.; Cong, C.; Shen, X.; Wu, X.; Yeow, E. K.; Yu, T. Nonblinking, intense two-dimensional light emitter: monolayer WS2 triangles. *ACS Nano* **2013**, *7*, 10985−10994.
(54) Choi, W.; Cho, M. Y.; Konar, A.; Lee, J. H.; Cha, G. B.; Hong, S. C.; Kim, S.; Kim, J.; Jena, D.; Joo, J.; et al. High-detectivity multilayer MoS2 phototransistors with spectral response from ultraviolet to infrared. *Adv. Mater.* **2012**, *24*, 5832−5836.
(55) Yin, Z.; Li, H.; Li, H.; Jiang, L.; Shi, Y.; Sun, Y.; Lu, G.; Zhang, Q.; Chen, X.; Zhang, H. Single-layer MoS2 phototransistors. *ACS Nano* **2012**, *6*, 74−80.
(56) Liang, F.-X.; Zhang, D.-Y.; Wang, J.-Z.; Kong, W.-Y.; Zhang, Z.-X.; Wang, Y.; Luo, L.-B. Highly sensitive UVA and violet photodetector based on single-layer graphene-TiO 2 heterojunction. *Opt. Express* **2016**, *24*, 25922−25932.
(57) Tsai, D.-S.; Liu, K.-K.; Lien, D.-H.; Tsai, M.-L.; Kang, C.-F.; Lin, C.-A.; Li, L.-J.; He, J.-H. Few-layer MoS2 with high broadband photogain and fast optical switching for use in harsh environments. *ACS Nano* **2013**, *7*, 3905−3911.
(58) Yao, J.; Zheng, Z.; Shao, J.; Yang, G. Stable, highly-responsive and broadband photodetection based on large-area multilayered WS 2 films grown by pulsed-laser deposition. *Nanoscale* **2015**, *7*, 14974−14981.
(59) Choi, M. S.; Qu, D.; Lee, D.; Liu, X.; Watanabe, K.; Taniguchi, T.; Yoo, W. J. Lateral MoS2 p−n junction formed by chemical doping for use in high-performance optoelectronics. *ACS Nano* **2014**, *8*, 9332−9340.
(60) Huang, Z.; Zhang, T.; Liu, J.; Zhang, L.; Jin, Y.; Wang, J.; Jiang, K.; Fan, S.; Li, Q. Amorphous MoS2 photodetector with ultra-broadband response. *ACS Appl. Electron. Mater.* **2019**, *1*, 1314−1321.
(61) Cui, S.; Mei, Z.; Zhang, Y.; Liang, H.; Du, X. Room-Temperature Fabricated Amorphous Ga2O3 High-Response-Speed Solar-Blind Photodetector on Rigid and Flexible Substrates. *Adv. Opt. Mater.* **2017**, *5*, No. 1700454.
(62) Guo, X.; Hao, N.; Guo, D.; Wu, Z.; An, Y.; Chu, X.; Li, L.; Li, P.; Lei, M.; Tang, W. H. Compounds, β-Ga2O3/p-Si heterojunction solar-blind ultraviolet photodetector with enhanced photoelectric responsivity. *J. Alloys Compd.* **2016**, *660*, 136−140.
(63) Garg, M.; Tak, B. R.; Rao, V. R.; Singh, R. interfaces, Giant UV photoresponse of GaN-based photodetectors by surface modification using phenol-functionalized porphyrin organic molecules. *ACS Appl. Mater. Interfaces* **2019**, *11*, 12017−12026.
(64) Singh, A.; Sharma, M.; Singh, R. Design, NaCl-Assisted CVD Growth of Large-Area High-Quality Trilayer MoS2 and the Role of the Concentration Boundary Layer. *Cryst. Growth Des.* **2021**, *21*, 4940−4946.

https://doi.org/10.1021/acsomega.1c06855
ACS Omega 2022, 7, 11731−11741